Nonlinear Evolution of the Multiple n Toroidicity-induced Alfvén Eigenmode

Yang Chen, Roscoe B. White

Princeton Plasma Physics Laboratory, P.O. Box 451, Princeton, New Jersey 08543

A numerical algorithm is established for studying the simultaneous excitation of multiple n TAE modes due to energetic particles. Each mode is described by its slowly-varying mode amplitude and phase, which evolve according to equations derived from the kinetic-MHD equation. A Hamiltonian guiding center code is used to simulate the alpha particle motion. The important effect of mode overlapping on the saturation level is demonstrated for the two modes, $n = 2$ and $n = 3$. Without other damping effects, a single mode saturates at a level where no significant overlapping occurs, while the excitation of multiple modes generally leads to resonance overlapping among different modes for typical β_h, which will eventually cause global particle loss.

PACS numbers: 52.35.-g 52.35.Py

1. Introduction

The saturation mechanisms of Toroidicity-Induced-Alfvén-Eigenmodes (TAE) are generally categorized into two groups, that due to MHD nonlinearity, in the form of distortions of linear mode structure and generation of Fourier modes outside the linearly unstable spectrum by nonlinear mode coupling effects , and that of nonlinear particle dynamics in a wave field, leading to such effects as particle trapping , stochastic motion and modification of the particle distribution. For low n modes this later mechanism is supported by recent hybrid kinetic-MHD simulations[1,2]. It is then possible to describe each mode by a fixed mode structure, with time-dependent (slowly-varying) amplitude and phase as a result of energetic-particle driving. By using such a reduced description of the background plasma one can afford to include all the important nonlinear particle dynamics in the numerical simulation, and study the parameter dependence of the saturation process, which is not possible in a fully nonlinear kinetic-MHD simulation.

The behavior of energetic particles in a wave field such as TAE has been a subject of extensive research. Of particular concern is whether the TAE amplitude becomes large enough to cause resonance overlapping, which can lead to global particle diffusion and energy loss. As shown previously[3], mode overlapping is greatly facilitated by the simultaneous excitation of multiple modes. For a single mode, only the resonance islands associated with that mode can overlap, therefore the modification of the particle distribution is relatively localized. When there are multiple modes, the resonance islands corresponding to different

modes might overlap, leading to a global modification of the particle distribution, hence greatly increasing the energy release of particles and the mode saturation amplitudes.

In this paper we present a general formalism for numerically investigating the simultaneous evolution of multiple TAEs, driven unstable by energetic particles . In Section 2 the equations for mode amplitudes and phases are derived from the linearized Kinetic-MHD equation. A numerical simulation scheme is established in Section 3, and in Section 4 we present the simulation results.

2. Equations

We start with the linearized current coupling equation[4,5],

$$\begin{aligned}\rho\frac{\partial^2\vec{\xi}}{\partial t^2} &= \hat{F}(\vec{\xi}) - (\vec{J}_h - q_h\frac{\partial\vec{\xi}}{\partial t})\times\vec{B} \\ &= \hat{F}(\vec{\xi}) + \vec{S}(\vec{x},t),\end{aligned} \tag{1}$$

where ρ is the bulk plasma density, $\vec{\xi}$ the plasma displacement, $\hat{F}$ the usual force operator, $\vec{J}_h$ and q_h the energetic particle current density and charge density; thus $\vec{S}$ stands for the energetic particle effect. The term $q_h\frac{\partial\vec{\xi}}{\partial t}\times\vec{B}$ can be interpreted as the Coulomb force on a charged bulk plasma(with charge density $-q_h$), in the electric field $\vec{E} = -\frac{\partial\vec{\xi}}{\partial t}\times\vec{B}$. We shall use perturbation analysis to find the leading behavior of $\vec{\xi}$. Consider the mode with eigenfrequency ω_n, for which the eigenmode structure is known to be $\vec{\eta}_n(\vec{x})$. Assume the solution of (1) is

$$\vec{\xi}(\vec{x},t) = A_n(t)\vec{\eta}_n(\vec{x})sin(\omega_n t + \alpha_n(t)) + \vec{\xi}_1, \tag{2}$$

where the amplitude $A_n(t)$, and phase $\alpha_n(t)$ are assumed to be slowly -varying, describing the evolution of the unstable mode due to the energetic particles. The quantity $\vec{\xi}_1$ is the deviation of the exact solution from the assumed slowly-varying main mode. We wish to choose $A_n(t)$ and $\alpha_n(t)$, such that the error part ξ_1 is as small as possible. Expand ξ_1 in terms of a set of normalized discrete eigenmodes of the operator $\hat{F}$, $\vec{\eta}_j(\vec{x}), j = 1, \cdots$, with eigenvalue ω_j^2,

$$\xi_1 = \sum_j a_j(t)\vec{\eta}_j(\vec{x}) \tag{3}$$

where $a_j(t)$ are the time-dependent coefficients. Substitute $\vec{\xi}(\vec{x},t)$ into Eq.(1), giving

$$\sum_j \rho(\frac{d^2 a_j}{dt^2} + \omega_j^2 a_j)\vec{\eta}_j = -2\omega_n \rho\vec{\eta}_n[\dot{A}_n cos(\omega_n t + \alpha_n) - A_n\dot{\alpha}_n sin(\omega_n t + \alpha_n)] + \vec{S}(\vec{x},t) \tag{4}$$

Since $A_n(t)$, $\alpha_n(t)$ are slowly-varying, terms contains d^2A_n/dt^2 ,$d^2\alpha_n/dt^2$,$\dot{A}_n \cdot \dot{\alpha}_n$ are neglected. Multiply both sides of (4) by η_i, integrate over space, and use the orthogonality of different eigenmodes of the operator $\hat{F}$, to find

$$\frac{d^2 a_i}{dt^2} + \omega_i^2 a_i = \int \vec{S}\cdot\vec{\eta}_i d^3\vec{r} - 2\omega_n[\dot{A}_n cos(\omega_n t + \alpha_n) - A_n\dot{\alpha}_n sin(\omega_n t + \alpha_n)]\cdot\delta_{in} \tag{5}$$

Since $\vec{\xi}_1$ is small compared with the main part $A_n sin(\omega_n + \alpha_n)$, $\vec{S}$ is essentially the response of the hot ions to the main mode. We now distinguish two time scales on the right-hand side of Eq.(5), namely, the fast time scale ω_n^{-1} and the slow time scale ω_t^{-1},

the wave-trapping time of particles. Apart from the small resonant region (compared with the whole phase space) of the hot ion distribution, whose response to the mode $\vec{\eta}_n$ is slowly-varying (with time scale ω_t^{-1}), the hot ion response is approximately linear, and we have $\int \vec{S} \cdot \vec{\eta}_i d^3\vec{r} \approx c_1(t)cos(\omega_n t) + c_2(t)sin(\omega_n t)$, with $c_1(t), c_2(t)$ slowly-varying. Thus among the equations for $a_i(t)$, only the equation for $a_n(t)$ has resonant drive terms on its R.H.S., all other $a_i's$ will stay small if they are initially small. However, the coefficient $a_n(t)$ will increase rapidly on the fast time scale ω_n^{-1}, quickly invalidating the approximate solution $A_n \cdot \vec{\eta}_n sin(\omega_n t + \alpha_n)$. This can be avoided if we choose $A_n(t)$ and $\alpha_n(t)$ such that the coefficients of $sin(\omega_n t)$ and $cos(\omega_n t)$ vanish on the fast time scale. Notice that these coefficients can be picked out by mutiplying (5) for $i = n$ by $sin(\omega_n t)$ and $cos(\omega_n t)$ alternatively and averaging the resulting equations over the fast time scale, giving the equations

$$< \int \vec{S} \cdot \vec{\eta}_n cos(\omega_n t) d^3\vec{r} > -\omega_n \dot{A}_n cos(\alpha_n) + A_n \omega_n \dot{\alpha}_n sin(\alpha_n) = 0 \tag{6}$$

$$< \int \vec{S} \cdot \vec{\eta}_n sin(\o 2mega_n t) d^3\vec{r} > +\omega_n \dot{A}_n sin(\alpha_n) + A_n \omega_n \dot{\alpha}_n cos(\alpha_n) = 0 \tag{7}$$

Where $< \cdots >$ indicates the time-average. Noting that the electric field corresponding to a displacement $\vec{\xi}$ is $-\partial\vec{\xi}/\partial t \times \vec{B}$, we have $\vec{E}_n(\vec{x}, t) = -A_n \cdot \omega_n \vec{\eta}_n \times \vec{B} \cdot cos(\omega_n t + \alpha_n)$. Defining the growth rate $\gamma_n = \dot{A}_n / A_n$, Eq.(6)-(7) can be rearranged in the following form,

$$\gamma_n = - < \int \vec{J}_h \cdot \vec{E}_n d^3\vec{r} > /(\omega_n^2 A_n^2) \tag{8}$$

$$\dot{\alpha}_n(t) = - < \int \vec{J}_h \cdot \frac{1}{\omega_n} \frac{\partial \vec{E}_n}{\partial t} d^3\vec{r} > /\omega_n^2 A_n^2 \tag{9}$$

The first equation just expresses the energy conservation of the coupled system. Generalization to the case of multiple n is trivial and Eqs. (8)-(9) still hold for each mode , with J_h always the energetic particle current in the total perturbed field. This equation is similar to the equation derived for a 1-D problem from Poisson's equation[6] and that for Alfvén wave problem from the Langrangian approach[7]. It can also be derived directly from the quadratic form corresponding to Eq.(1).

Energetic particles are described by the drift-kinetic equation for the guiding center distribution $f(\vec{r}, \varepsilon, \mu, t)$, $\varepsilon = \frac{1}{2}mv^2$,

$$\frac{\partial f}{\partial t} + \vec{V}_G \cdot \nabla f + q\vec{E} \cdot \vec{V}_G \frac{\partial f}{\partial \varepsilon} = 0 \tag{10}$$

here $\vec{V}_G(\vec{r}, \varepsilon, \mu, t)$ is the guiding center velocity, q the particle charge. The energy change of a particle includes a term $\mu\frac{\partial B}{\partial t}$ which is neglected here as an effect of second order in the perturbation, since for the Alfvén wave $\delta\mathbf{B}$ is mainly perpendicular . We shall use the nonlinear δf method[8–11] to simulate particles. Writing $f = f_0 + \delta f$, where f_0 is the equilibrium distribution, δf the perturbed distribution, we have, along particle trajectories,

$$\frac{d\delta f}{dt} = -\vec{V}_{G1} \cdot \nabla f_0 - q\vec{E} \cdot \vec{V}_G \frac{\partial f_0}{\partial \varepsilon} \tag{11}$$

here $\vec{V}_{G1}$ is the perturbed guiding center velocity.

Using f or δf, the equations for γ_n and $\dot{\alpha}_n$ are,

$$\gamma_n = - < \int q\vec{V}_G \cdot \vec{E}_n f d\tau > /(\omega_n^2 A_n^2) \tag{12}$$

$$\dot{\alpha}_n = - < \int q\vec{V}_G \cdot \frac{1}{\omega_n}\frac{\partial \vec{E}_n}{\partial t} f d\tau > /(\omega_n^2 A_n^2) \tag{13}$$

Here $d\tau = d^3\vec{r}d^3\vec{v}$. The contributions to γ_n and $\dot{\alpha}_n$ from f_0, γ_{n0} and $\Delta\omega$, are constants and can be calculated once and for all,

$$\gamma_n = \gamma_{n0} - < \int q\vec{V}_G \cdot \vec{E}_n \delta f d\tau > /(\omega_n^2 A_n^2) \tag{14}$$

$$\dot{\alpha}_n = \Delta\omega - < \int q\vec{V}_G \cdot \frac{1}{\omega_n}\frac{\partial \vec{E}_n}{\partial t}\delta f d\tau > /(\omega_n^2 A_n^2) \tag{15}$$

Since $\Delta\omega$ is just a constant, it will be absorbed into ω_n. On the other hand, γ_{n0} is found to be neglegible for a mode with $E_\parallel = 0$, hence it will be dropped in the following.

As is clear from Eq.(10), we are here neglecting any particle source or sink or classical relaxation process, which, depending on the characteristic parameters, can change dramatically the long time behavior of the driven system[3]. In effect, we are considering the system on the wave-trapping time scale. Ion Landau-damping can be included by changing particle loading, other damping effects (electron Landau-damping, electron collisional damping, continuum damping, etc., see Fu *et al.*[12] and references therein) can be included here as an effective damping rate added to γ_n. In the simulation presented here all these damping effects are set to zero.

3. Simulation Technique

A Hamiltonian guiding center code[13] *ORBIT* is used to follow the particle trajectories. Here and in the following we use the major radius as the unit of length, inverse on-axis gyrofrequency as the unit of time. The magnetic field is $\vec{B} = g\nabla\phi + I\nabla\theta$, where g and I

are related to the poloidal and toroidal current. The guiding-center Hamiltonian is

$$\mathcal{H} = \frac{1}{2}\rho_{\parallel}^2 B^2 + \mu B + \Phi \tag{16}$$

with four Hamiltonian variables

$$\phi,\ \theta,\ P_\phi = g\rho_c - \psi_p,\ P_\theta = I\rho_c + \psi_t \tag{17}$$

where $\rho_c = \rho_{\parallel} + \tilde{\alpha}, \rho_{\parallel} = v_{\parallel}/B$, ψ_t is the toroidal flux with $d\psi_t/d\psi_p = q$, Φ is the electric potential and $\tilde{\alpha}$ gives the magnetic perturbation through $\delta\mathbf{B} = \nabla \times \tilde{\alpha}\mathbf{B}$. The guiding center equations are[13]

$$\dot{P}_\phi = -\frac{\partial \mathcal{H}}{\partial \phi}, \qquad \dot{\phi} = \frac{\partial \mathcal{H}}{\partial P_\phi} \tag{18}$$

$$\dot{P}_\theta = -\frac{\partial \mathcal{H}}{\partial \theta}, \qquad \dot{\theta} = \frac{\partial \mathcal{H}}{\partial P_\theta} \tag{19}$$

It is also easy to find the radial drift

$$\dot{\psi}_p = \frac{g}{D}\dot{P}_\theta - \frac{I}{D}\dot{P}_\phi \tag{20}$$

and the parallel acceleration

$$\dot{\rho}_{\parallel} = \frac{1}{g}(\dot{P}_\theta + \dot{\psi}_p) - (P_\theta + \psi_p)\frac{g'}{g^2}\dot{\psi}_p - \dot{\tilde{\alpha}} \tag{21}$$

where

$$\dot{\tilde{\alpha}} = \dot{\theta}\frac{\partial \tilde{\alpha}}{\partial \theta} + \dot{\psi}_p\frac{\partial \tilde{\alpha}}{\partial \psi_p} + \dot{\phi}\frac{\partial \tilde{\alpha}}{\partial \phi} + \frac{\partial \tilde{\alpha}}{\partial t} \tag{22}$$

and $D = gq + I + \rho_{\|}(gI' - Ig')$.

The quantity $\tilde{\alpha}$ in the numerical code is represented as

$$\tilde{\alpha}(\psi_p, \theta, \phi, t) = \sum_{nm} A_n(t)\tilde{\alpha}_{nm}(\psi_p) sin(n\phi - m\theta - \omega_n t - \alpha_n(t)) \tag{23}$$

and the electric potential Φ is calculated through the condition $E_{\|} = 0$,

$$\vec{b} \cdot (-\nabla\Phi - \frac{\partial\tilde{\alpha}}{\partial t}\mathbf{B}) = \mathbf{0} \tag{24}$$

with $\vec{b} = \mathbf{B}/B$. The mode structure $\tilde{\alpha}(\psi_p)$ used in this paper is generated by the *NOVA* code[14].

We load pseudo-particles in the 5-D space $(\varepsilon, \lambda, \psi_p, \theta, \phi)$ ($\lambda = v_{\|}/v$ is the pitch) such that we can assign to each particle j a phase space volume element τ_j in an obvious way. For example, we can load particles on a uniform grid, then $\tau_j = J_j \varepsilon^{\frac{1}{2}}$, where J is the Jacobian such that $d^3\vec{r} = Jd\psi_p d\theta d\phi$. As a particle moves in phase space, the shape of its associated volume element will be deformed, but the volume is constant, due to the Hamiltonian nature of the motion. By integrating the guiding center equations together with the equation for δf, we have a representation of δf at particle positions, the integrals in Eq.(14)-(15) are then written as sums over particles,

$$\gamma_n = - < \frac{1}{\omega_n^2 A_n^2} \sum_j \delta f_j \vec{E}_n(j) \cdot \vec{V}_G(j)\tau_j > \tag{25}$$

$$\dot{\alpha}_n = - < \frac{1}{\omega_n^2 A_n^2} \sum_j \delta f_j \frac{1}{\omega_n} \frac{\partial \vec{E}_n}{\partial t}(j) \cdot \vec{V}_G(j)\tau_j > \tag{26}$$

Wave amplitudes and phases are then advanced according to these equations each step.

This scheme of updating the wave amplitude is different from that used before[11], where explicit energy conservation was used. We find that the present method significantly reduces the noise level.

We have tried to avoid using the δf method in favor of more conventional particle simulation methods such as the weighted-particle scheme. The latter is desirable if one wants to extend the simulation to longer time scales where the effect of particle source and sink is important, as the pulsation of the energetic particle population might dominate on that time scale. At present we find the δf method is crucial for resolving the 5-D phase space.

4. Numerical Results and Discussion

We consider the simultaneous evolution of the $n = 2$ and $n = 3$ modes, and for each n only the two most important poloidal harmonics are included, thus the harmonics we considered are $(n, m) = (2, 2)$,$(2, 3)$, $(3, 3)$,$(3, 4)$. For simplicity an analytic equlibrium with circular flux surfaces[13] is used. The equilibrium particle distribution is assumed to be $f_0(r, \varepsilon) = e^{-r^2/\delta r^2} \varepsilon^{-\frac{3}{2}}$. In the following simulation we use ITER-like parameters: $R = 800cm$, $a = 300cm$, $B = 6T$, $\delta r = a/3$, mode frequencies are $\omega_{n=3}/\Omega_c = 1.34 \times 10^{-3}$, $\omega_{n=2}/\Omega_c = 1.12 \times 10^{-3}$ where Ω_c is the on-axis gyro-frequency. Mode structures and q-profile used are shown in Fig. 1.

It is helpful to analyze the layout of resonance locations in the phase space. The

precise resonance condition involves action-angle variables for guiding center motion[15], but for far-passing particles it has the simple form,

$$n\dot{\phi}(t) - l\dot{\theta}(t) - \omega_n = 0 \tag{27}$$

here l is an integer, $\phi(t)$ and $\theta(t)$ are the unperturbed motion. Corresponding to each harmonic (n, m) there are two important resonances, with $(n, l) = (n, m-1)$ and $(n, m+1)$ respectively. Note that Eq.(27) is independent of ϕ but weakly dependent on θ. For given μ and θ Eq.(27) defines a resonance curve in $r - \rho_\parallel$ plane for each (n, l) (a torus in $(r, \rho_\parallel, \phi)$ space). The possible (n, l) pairs for our problem are $(2,1)$, $(2,2)$,$(2,3)$,$(2,4)$,$(3,2)$,$(3,3)$,$(3,4)$,$(3,5)$, and the corresponding resonance curves for $\mu = 0$, $\theta = 0.1$ are plotted in Fig. 2. Since we need only consider those particles with energy above a threshold (about one third of the alpha birth energy), and since the high energy particle population decreases rapidly in minor radius, the most important resonances are $(n, l) = (2,2)$,$(2,3)$,$(3,3)$, $(3,4)$.

We can make a Poincaré plot of a particle (with $\mu = 0$) trajectory in this $r - \rho_\parallel$ plane, by registering its $(r, \rho_\parallel)$ value as a point whenever the particle passes $\theta = 0.1$. Without a perturbation the plot consists of a single point, with the perturbation the Poincaré points for a near resonant particle will spread up, mainly along the radius. The radial excursion of Poincaré points increases with increasing wave amplitude. When the radial excursion reaches the distance between two resonance curves, resonance overlapping occurs. In Fig. 2 are shown two Poincaré plots, one for a co-moving particle, the other for a counter-moving

particle, both with initial energy $\varepsilon = 3.7Mev$, $\theta = 0.1$, and $\phi = 0.$. The amplitudes are $A_{n=3} = A_{n=2} = 5 \times 10^{-5}$. Our normalization is such that the actual peak value of $\delta \mathbf{B}_r$ is about 10 times the amplitude used. The same particles are replotted in Fig. 3, but with $A_{n=3} = A_{n=2} = 10^{-4}$. We can see in the first case no overlapping occurs, while in the second case there is overlapping. Notice that the overlapping resonances come from different modes. By changing the initial positions of the particles in the plane and observing the changes in the Poincaré plot, we find that particles with higher energy tend to have larger radial excursion, and overlapping occurs first for those particles, when the amplitudes are around 10^{-4}. In the simulation particles are loaded uniformly in pitch-angle, and we find that the trapped particle contribution to the linear growth rate is not neglegible, although small compared with the passing particle contribution. Such a particle distribution makes the phase space resonance structure much more complicated, and the onset of resonance overlapping more difficult to predict. Nevertheless, we expect the onset of overlapping for far-passing particles will play a prominent role in the multiple mode evolution.

Poincaré plots can also be used to measure the wave-trapping time numerically. It has been shown[16,11] that the quantity $Q_{nl} = n\phi - l\theta - \omega_n t$ for a particle near resonance goes through pendulum motion, the frequency of which defines the wave-trapping frequency. We can make a Poincaré plot in the $r - Q_{nl}$ plane, for the trajectory of a particle deeply trapped in the wave. The wave-trapping period can be measured by adjusting the run

time such that the Poincaré points just trace a closed curve, as the one shown in Fig. 4 for $(n,l) = (3,3)$, $A_{n=3} = 1. \times 10^{-4}$, the trapping time is measured to be $\tau_{trap} = 105\tau_{tran}$ (τ_{tran} is the transit time defined by $\tau_{tran} = 2\pi R/v_{\parallel}$ for a typical $v_{\parallel}$), or $\tau_{trap}\omega_{n=3} = 157$.

From Fig. 2 we see for single mode overlapping (such as that between $(n,l) = (3,3)$ and $(3,4)$) to occur, particle radial excursion has to be larger compared with that necessary for overlapping between different toroidal modes. In our case the volume-averaged energetic particle β is $\beta_h \leq 3. \times 10^{-3}$ and no overlapping occurs for single mode saturation (again only far-passing particles are considered), hence the distribution flattening that leads to single mode saturation happens in well-isolated islands and on a well-defined time scale, namely the wave-trapping time corresponding to each island. As overlapping occurs in the multiple mode case, the particle distribution flattens in an enlarged region, leading to increased energy release and saturation amplitudes. But as a result of chaotic behavior of particle dynamics in the overlapping region, the evolution scenario is more complicated. Often in the simulation it is difficult to tell whether the modes have saturated , and this is complicated by the growing noise level which eventually gives problems. In the following we choose the run time such that the final growth rate is much smaller than the instantaneous wave-trapping frequency (which is comparable to the linear growth rate), typically in the range of $4 - 10\tau_{trap}$ with τ_{trap} as measured above. Fig. 5 plots the simultaneous saturation of the two modes for $\beta_h = 2. \times 10^{-3}$, with a run time of $700\tau_{tran}$, and 25900 particles loaded. The growth rate and frequency shift are shown in Fig. 6 and Fig. 7. The

frequency shift is approximately a constant and can largely be revealed from linear analysis, no phase change correlated with nonlinear development is observed. The effect of the remaining phase fluctuation is found to be small. Final amplitudes are $A_{n=3} = 6.4 \times 10^{-4}$ and $A_{n=2} = 2.2 \times 10^{-4}$, linear growth rates are $\gamma_{n=3}/\omega_{n=3} = 0.011$ and $\gamma_{n=2}/\omega_{n=2} = 0.012$. In another run the number of particles is increased to 259000, but the result is not significantly changed. From Fig. 6 we see that at the final stage the noise in the growth rate is overwhelming, this is true especially for large final amplitudes. Longer run time is practically prohibited by the growing noise level.

We now change β_h as a parameter, to control the saturation amplitude. For each β_h, we first run the two modes separately, then run the two modes simultaneously. At low β_h the saturation amplitudes are too small to cause resonance overlapping, and we expect the evolution of each mode will not be changed by the presence of the other . As β_h (hence saturation level) is increased, the width of each resonance island is increased, eventually leading to island overlapping and significant change in the amplitude evolution. Numerical results of the final amplitude for $n = 3$ vs. β_h is shown in Fig. 8. Initial amplitudes are 10^{-6} for both modes. Notice that for a single mode the saturation level $A^{1/2}$ is approximately linear in β_h, demonstrating the well-known result that at saturation the wave-trapping frequency (proportional to $A^{1/2}$) scales linearly with the linear growth rate (proportional to β_h). Apparent deviation between the amplitudes starts around $\beta_h = 1.6 \times 10^{-3}$, where $A_{n=3} \approx 0.78 \times 10^{-4}$ when run separately and $A_{n=3} \approx 1.0 \times 10^{-4}$ when run simultaneously.

At $\beta_h = 1.83 \times 10^{-3}$ the amplitude for the single mode is 1.02×10^{-4}, and 2.40×10^{-4} for the double mode run, indicating significant mode overlapping. This is consistent with the previous analysis of particle trajectories. The amplitude for simultaneous excitation is drastically increased at large β_h. Global particle loss is not seen on the simulation time scale for the two modes considered here. The study of large numbers of toroidal modes requires more simulation particles to resolve the phase space, and is therefore limited by computing power. It can be expected however, based on the results of two modes, that without other damping effects global particle loss will eventually set in as more modes are excited.

5. Conclusion

A numerical algorithm is established for studying the simultaneous excitation of multiple n TAE modes due to energetic particles. Each mode is described by its slowly-varying mode amplitude and phase, which evolve according to equations derived from the kinetic-MHD equation. Energetic particles are described by the drift-kinetic equations, where all the important particle dynamics are retained. Although a simple low-β equilibrium is used in this paper, the formalism is general enough for studying realistic plasmas. The important effect of mode overlapping on the saturation level is demonstrated for the two modes, $n = 2$ and $n = 3$. Without other damping effects, a single mode saturates at a level where no significant overlapping occurs, while the excitation of multiple modes generally leads to

resonance overlapping among different modes for typical β_h, which will eventually cause global particle loss. To compare the simulation results with the experiments, damping effects must be carefully studied and included.

ACKNOWLEDGMENTS

The authors are grateful to Dr. G. Y. Fu for helpful discussions. This work was supported by the U.S. Department of Energy under contract number DE-AC02-76-CHO3073.

---

1. G.Y.Fu and W.Park, Phys. Rev. Lett. **74**, 1594 (1995).

2. Y.Todo, T.Sato, K.Watanabe, and R.Horiuchi, Phys. Plasmas **2**, 2711 (1995).

3. H. L. Berk, B. N. Breizman, and H. Ye, Phys. Rev. Lett. **68**, 3563 (1992).

4. W. Park, S. Parker, H. Biglari, M. Chance, L. Chen, C. Z. Cheng, T. S. Hahm, W. W. Lee, R. Kulsrud, D. Monticello, L. Sugiyma, and R. B. White, Phys. Fluids B **4**, 2033 (1992).

5. R.Betti and J.P.Freidberg, Phys. Fluids B **3**, 538 (1991).

6. C.E.Rathmann, J.L.Vomvoridis, and J.Denavit, J. Comput. Phys. **26**, 408 (1978).

7. M.Pekker, H.L.Berk, B.N.Breizman, and J.Candy, Bull. Am. Soc. **40**, 1684 (1995).

8. S. Parker and W. W. Lee, Phys. Fluids B **5**, 77 (1993).

9. A. M. Dimits and W. W. Lee, J. Comput. Phys. **107**, 309 (1993).

10. M. Kotschenruether, Bull. Am. Phys. Soc. **34**, 2107 (1988).

11. Y. Wu, R. B. White, Y.Chen, and M.N.Rosenbluth, Phys. Plasmas **2(12)**, 4555 (1995).

12. G. Y. Fu, C. Z. Cheng, and K. L. Wong, Phys. Fluids B **5**, 4040 (1993).

13. R. B. White and M. S. Chance, Phys. Fluids **27**, 2455 (1984).

14. C. Z. Cheng, Phys. Reports **211**, 1 (1992).

15. A.N.Kaufman, Phys. Fluids **15**, 1063 (1972).

16. H. L. Berk, B. N. Breizman, and H. Ye, Phys. Fluids B **5**, 1506 (1993).

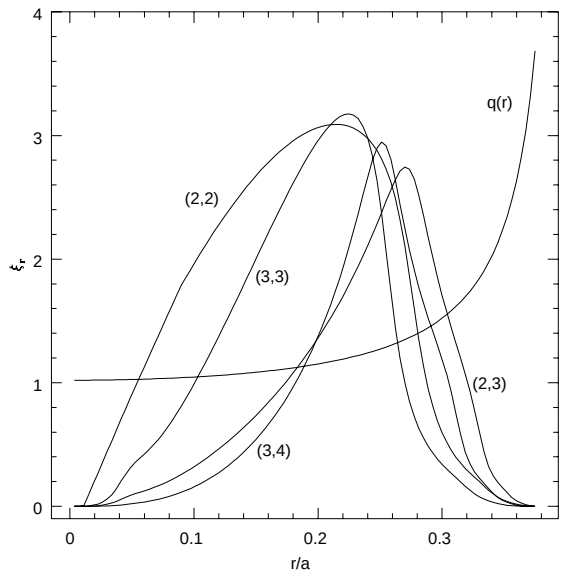

Fig. 1. q-profile and mode structures, labeled by toroidal and poloidal mode numbers (n, m)

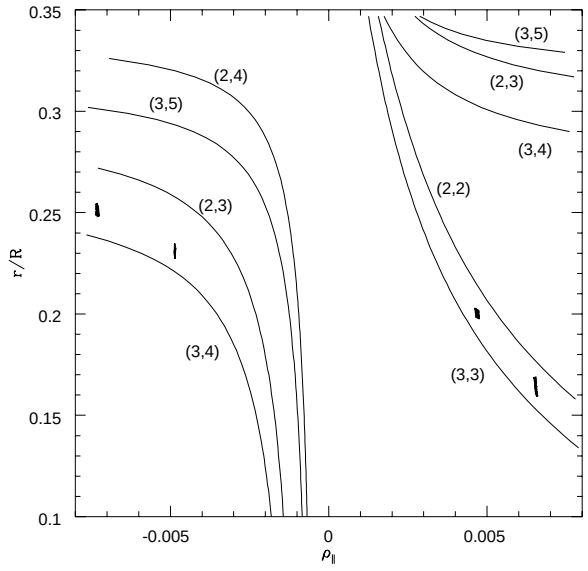

Fig. 2. Resonance curves for $\mu = 0$, $\theta = 0.1$, and Poincaré plots of particle trajectories for $A_{n=3} = A_{n=2} = 5 \times 10^{-5}$

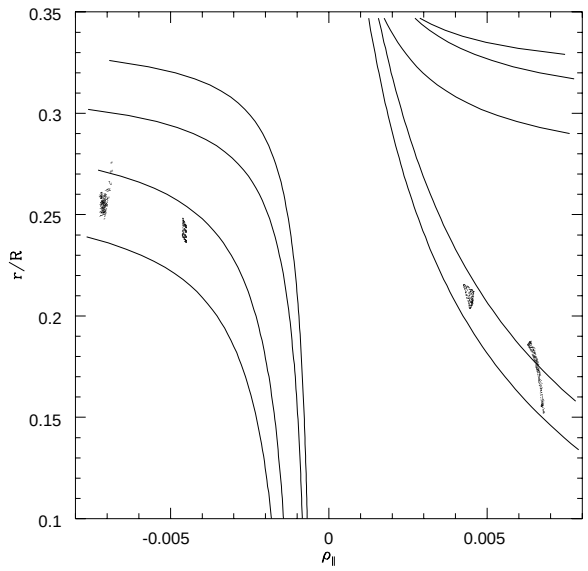

Fig. 3. Poincaré plots of particle trajectories for $A_{n=3} = A_{n=2} = 1. \times 10^{-4}$

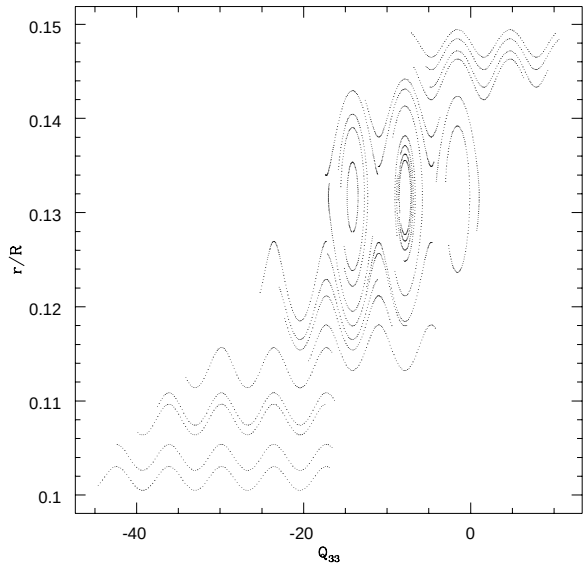

Fig. 4. Trapped and passing particle trajectories in a single n perturbation

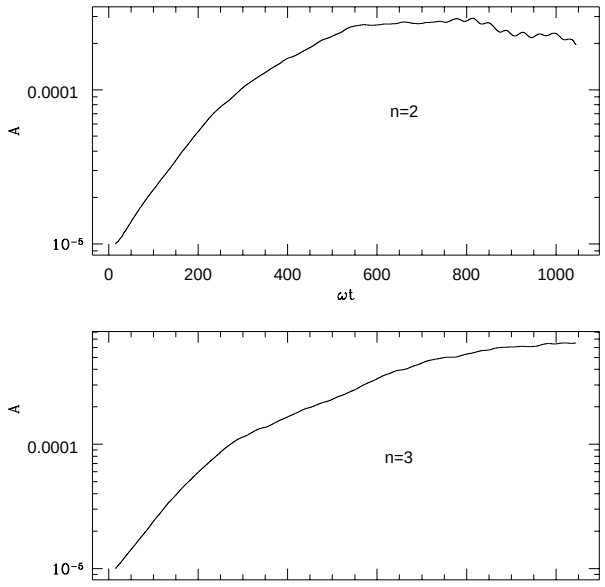

Fig. 5. The simultaneous evolution of two modes

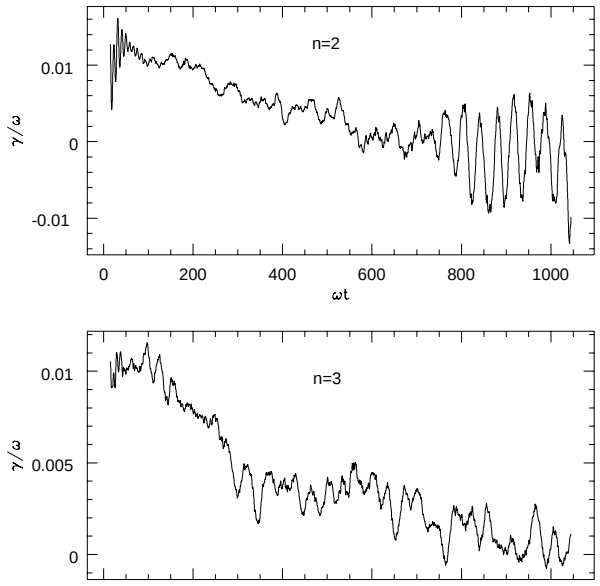

Fig. 6. Mode growth rates vs. time

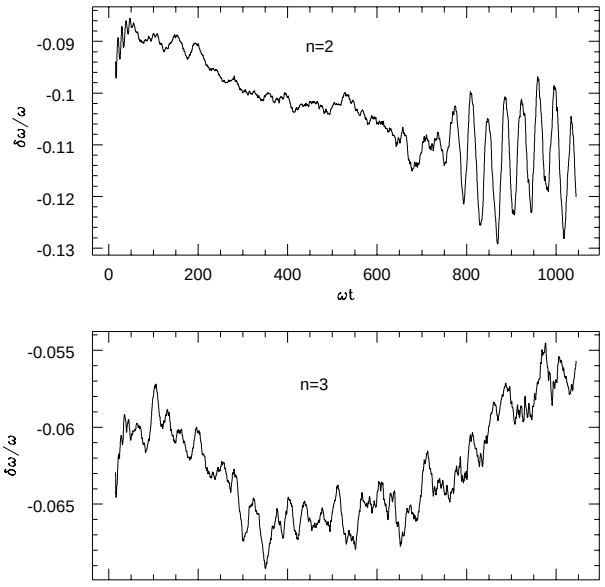

Fig. 7. Mode phase variation(frequency shift) vs.time

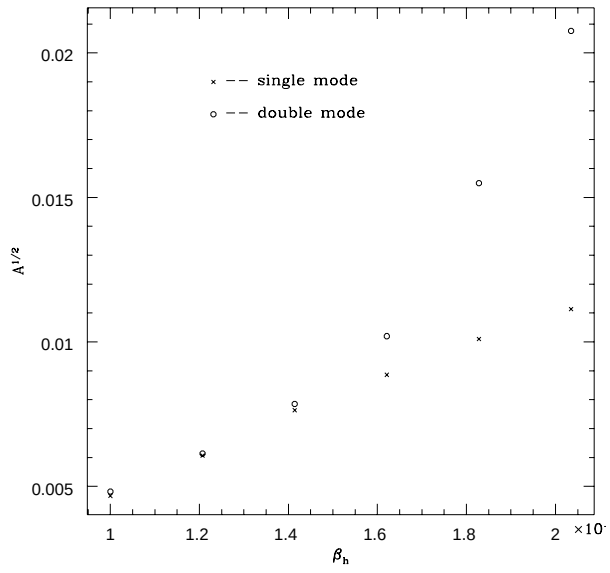

Fig. 8. Final amplitudes vs. β_h for $n = 3$.